2018

Chalcones and five-membered heterocyclic isosteres bind to alpha synuclein fibrils in vitro

Chia-Ju Hsieh
University of Pennsylvania

Kuiying Xu
University of Pennsylvania

Iljung Lee
University of Pennsylvania

Thomas J. A. Graham
University of Pennsylvania

Zhude Tu
Washington University School of Medicine in St. Louis

See next page for additional authors

ACS OMEGA

Article

Cite This: ACS Omega 2018, 3, 4486−4493

Chalcones and Five-Membered Heterocyclic Isosteres Bind to Alpha Synuclein Fibrils in Vitro

Chia-Ju Hsieh,[†] Kuiying Xu,[†] Iljung Lee,[†] Thomas J. A. Graham,[†,⊥] Zhude Tu,[‡] Dhruva Dhavale,[§] Paul Kotzbauer,[§] and Robert H. Mach*[,†,∥]

[†]Department of Radiology, University of Pennsylvania School of Medicine, Philadelphia, Pennsylvania 19104, United States

[‡]Mallinckrodt Institute of Radiology and [§]Department of Neurology, Washington University School of Medicine, St. Louis, Missouri 63110, United States

Supporting Information

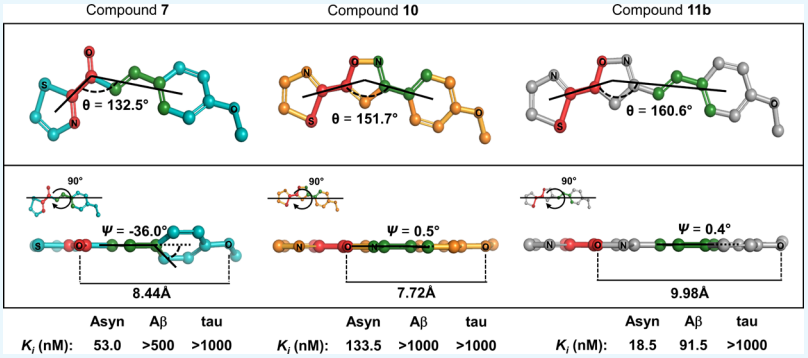

ABSTRACT: A series of chalcone and heterocyclic isosteres, in which the enone moiety was replaced with an isoxazole and pyrazole ring system, was synthesized and their affinities for alpha synuclein (Asyn), amyloid beta (Aβ), and tau fibrils were measured in vitro. The compounds were found to have a modest affinity and selectivity for Asyn versus Aβ fibrils and low affinity for tau fibrils. Insertion of a double bond to increase the extendable surface area resulted in an increase in affinity and improvement in selectivity for Asyn versus Aβ and tau fibrils. The results of this study indicate that compound **11** is a secondary lead compound for structure−activity relationship studies aimed at identifying a suitable compound for positron emission tomography-imaging studies of insoluble Asyn aggregates in Parkinson's disease.

INTRODUCTION

The accumulation of insoluble protein aggregates is the hallmark feature of most neurodegenerative disorders. For example, Alzheimer's disease (AD) is characterized by the formation of two different protein aggregates, amyloid plaques and neurofibrillary tangles (NFTs).[1] Amyloid plaques are formed by the misprocessing amyloid precursor protein to form Aβ1-42, and the misfolding of this protein from an alpha helix to a beta pleated sheet causes aggregation to form fibrils, which precipitate in the form of amyloid beta (Aβ) plaques. NFTs are caused by the fibrillization of hyperphosphorylated tau, a microtubule-associated protein, which is thought to be formed later in the disease process than Aβ plaques. For many decades, the identification of patients having AD was not confirmed until autopsy, a diagnosis that was based on the density of amyloid plaques and NFTs in various brain regions. There was a breakthrough in the clinical characterization of AD with the development of radiotracers such as [^{11}C]PiB and [^{18}F]-florbetapir, which are capable of providing a measure of amyloid plaques in living human brain in conjunction with positron emission tomography (PET).[2−4] More recent efforts have focused on the development of PET radiotracers for imaging aggregated tau in NFTs, and PET-imaging studies have confirmed that NFTs are formed much later in the disease process than Aβ plaques.[5−7]

A second neurodegenerative disease characterized by insoluble protein aggregates is Parkinson's disease (PD). In this case, the protein alpha synuclein (Asyn), a highly abundant protein in brain, is not degraded and leads to a similar formation of beta pleated sheets and fibril formation. The Asyn fibrils eventually form two different insoluble protein aggregates, Lewy bodies and Lewy neurites, which have been used to characterize PD at the time of autopsy.[8−10] Lewy bodies and Lewy neurites are also found in another Parkinsonian-like syndrome termed dementia with Lewy bodies and in glial cell inclusion bodies in multiple system atrophy. Taken collectively, these neurodegenerative disorders have been termed "synucleinopathies" because they have as a common feature the formation of insoluble protein aggregates of fibrillary Asyn.[11]

Received: November 30, 2017
Accepted: February 22, 2018
Published: April 24, 2018

DOI: 10.1021/acsomega.7b01897
ACS Omega 2018, 3, 4486−4493

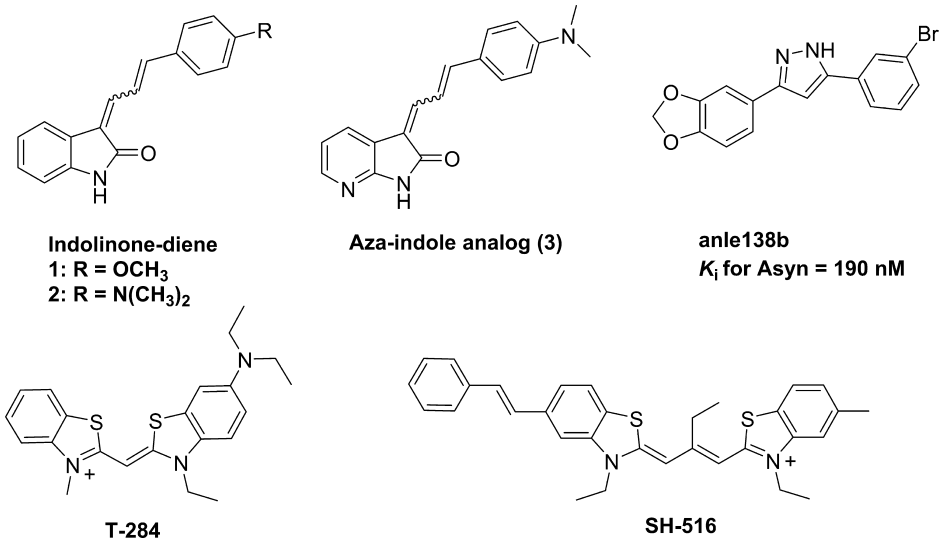

Figure 1. Structure of compounds reported to bind to Asyn fibrils.[13,16]

Scheme 1. Synthesis of Chalcone Analogues[a]

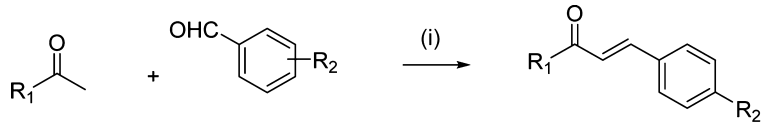

4 R_1 = 2-benzothiazolyl, R_2 = OCH_3
5 R_1 = 2-benzothiazolyl, R_2 = $N(CH_3)_2$
6 R_1 = 2-benzothiazolyl, R_2 = NO_2
7 R_1 = 2-thiazolyl, R_2 = OCH_3
8 R_1 = 2-thiazolyl, R_2 = $N(CH_3)_2$
9 R_1 = 2-thiazolyl, R_2 = NO_2

[a]Reagents and conditions: (i) NaOH, CH_3OH.

The tremendous success in the application of Aβ and tau imaging agents in the study of AD has led to an international effort to develop a PET radiotracer for imaging Asyn aggregates in Lewy bodies, Lewy neurites, and glial cell inclusion bodies. A limitation in the development of PET radiotracer for this purpose has been the dearth of lead compounds to serve as a starting point for structure−activity relationship (SAR) studies aimed at developing an optimized probe for translational imaging studies. Because Aβ and tau pathologies are often observed in postmortem samples of PD brain, it is important that a PET radiotracer for imaging Lewy bodies and Lewy neurites displays high selectivity for aggregated Asyn versus Aβ and tau.[12] This topic has been discussed in greater detail in a recent review.[11]

We previously reported the synthesis and in vitro characterization of a panel of indolinone−diene analogues as potent and selective ligands for Asyn versus Aβ and tau fibrils.[13] A limitation of this class of compounds is the tendency of some of the analogues to isomerize into E,E and Z,E isomers and their high lipophilicities, which limits their utility as a radioligand for PET-imaging studies.

For the current study, we chose to investigate a series of chalcone derivatives because the enone moiety serves as an isosteric replacement of the diene group while avoiding the E,E and Z,E isomerization problem observed with the indolinone−diene analogues. Chalcone analogues have been previously reported to bind to Aβ but had a low affinity for Asyn.[14,15] We also replaced the indole ring system with a benzothiazole ring system because our previous SAR study revealed that an electron-deficient ring such as the aza-indole system has a higher affinity for Asyn fibrils relative to the indole ring system (Figure 1; **1**−**3**).[13] The benzothiazole ring system is also present in cyanine dyes that have been shown to bind to Asyn fibrils (Figure 1; **T-284** and **SH-516**).[16] Finally, we replaced the enone moiety with an isoxazole and pyrazole ring system to avoid the Michael-acceptor properties of the chalcone system. We utilized thioflavin T (ThioT) competition assays to characterize the binding affinity, an approach we previously utilized for phenothiazine and indolinone−diene compounds to guide the identification of lead compounds for radiolabeling and further characterization.[13,17,18] The results of in vitro binding studies led to the identification of compounds having a higher affinity for Asyn versus Aβ and tau fibrils. Molecular-modeling studies were also conducted to identify the properties of the ligands contributing to this selectivity. Although the compounds described in this report do not have the high affinity to serve as a PET radiotracer for in vivo imaging studies, they could serve as secondary lead for further SAR studies.

RESULTS AND DISCUSSION

The synthesis of the target compounds involved a simple condensation reaction with 2-acetylbenzothiazole and the substituted benzaldehyde (Scheme 1). We chose to explore only the 4-OCH_3, 4-$N(CH_3)_2$, and 4-NO_2 substituted

DOI: 10.1021/acsomega.7b01897
ACS Omega 2018, 3, 4486−4493

compounds because our previous studies indicated that these were preferred substituents in the indolinone−diene series.[13] In vitro binding studies revealed that the benzothiazole chalcone analogues had only a modest affinity for Asyn fibrils and a slightly higher affinity for Aβ fibrils (Table 1 and Supporting Information Table). The calculated log *P* values were also higher than those of the corresponding indolinone−diene analogues, which is also an undesirable property for a PET radiotracer for brain-imaging studies.

Table 1. K_i Values (nM) of Chalcone Derivatives for Asyn, Aβ, and Tau Fibrils[a]

#	Asyn	Aβ	tau	log P[b]
1[c]	61.1 ± 9.6	125.8 ± 42.6	169.0 ± 22.3	3.1
2[c]	40.7 ± 8.7	27.6 ± 4.8	53.7 ± 9.7	3.5
3[c]	11.5 ± 2.0	15.3 ± 5.5	35.0 ± 12.3	2.9
4	530.5 ± 64.3	353.0 ± 29.7	716.5 ± 58.7	4.3
5	906.0 ± 29.7	91.0 ± 12.7	NB	4.2
6	>500	89.0 ± 26.9	NB	4.3
7	53.0 ± 19.8	>500	>1000	2.9
8	95.5 ± 29.0	505.0 ± 49.5	401.5 ± 118.1	3.3
9	191.5 ± 3.5	404.0 ± 80.6	NB	2.5

[a]Graphs for the ThioT competition binding assays are shown in the Supporting Information Table. [b]Calculated by ChemDraw Professional 15.1. [c]Compounds **1**−**3** are compounds **19**−**21** of Chu et al.[13]

The next step in the process involved removal of the benz-fused aromatic ring to make the corresponding thiazole chalcone analogues (**7**, **8**, and **9**; Scheme 1). We were quite surprised to see that this simple change in structure resulted in an increase in affinity for Asyn and improved selectivity for Asyn versus Aβ and tau fibrils. Of the three derivatives, the 4-methoxy group had the highest potency for Asyn (K_i = 53 nM) and the highest selectivity for Asyn versus Aβ and tau fibrils.

The isosteric replacement of the enone moiety of compound **7** with a five-membered heterocyclic ring was also explored. The rationale for this substitution was the publication of the pyrazole analogue, **anle138b** (Figure 1), which was reported to have a modest affinity for Asyn fibrils.[19,20] Therefore, both the pyrazole and isoxazole analogues of compound **7** were synthesized and evaluated in vitro for binding to Asyn, Aβ, and tau fibrils (Scheme 2). The results of in vitro binding studies revealed that the pyrazole (**12**) and isoxazole (**10**) analogues had an affinity for Asyn similar to that reported for **anle138b** (K_i = 190 nM) and good selectivity versus Aβ and tau fibrils (Table 2). As a final structural change, a double bond was inserted between the central heterocyclic ring system and the 4-methoxyphenyl ring. The synthesis of the target compounds is shown in Scheme 2. Although the synthesis of the pyrazole analogue resulted in the formation of a single isomer (**13**), the

Table 2. K_i Values (nM) of Isoxazole and Pyrazole Derivatives for Asyn, Aβ, and Tau Fibrils

#	Asyn	Aβ	tau	log P[a]
10	133.5 ± 78.5	>1000	>1000	3.03
11a,b	18.5 ± 9.2	91.5 ± 58.7	>1000	3.54
12	162.5 ± 41.7	>1000	>1000	2.95
13	59.0 ± 11.3	327.0 ± 76.4	>1000	3.47

[a]Calculated by ChemDraw Professional 15.1.

Scheme 2. Synthesis of Isoxazole and Pyrazole Analogues[a]

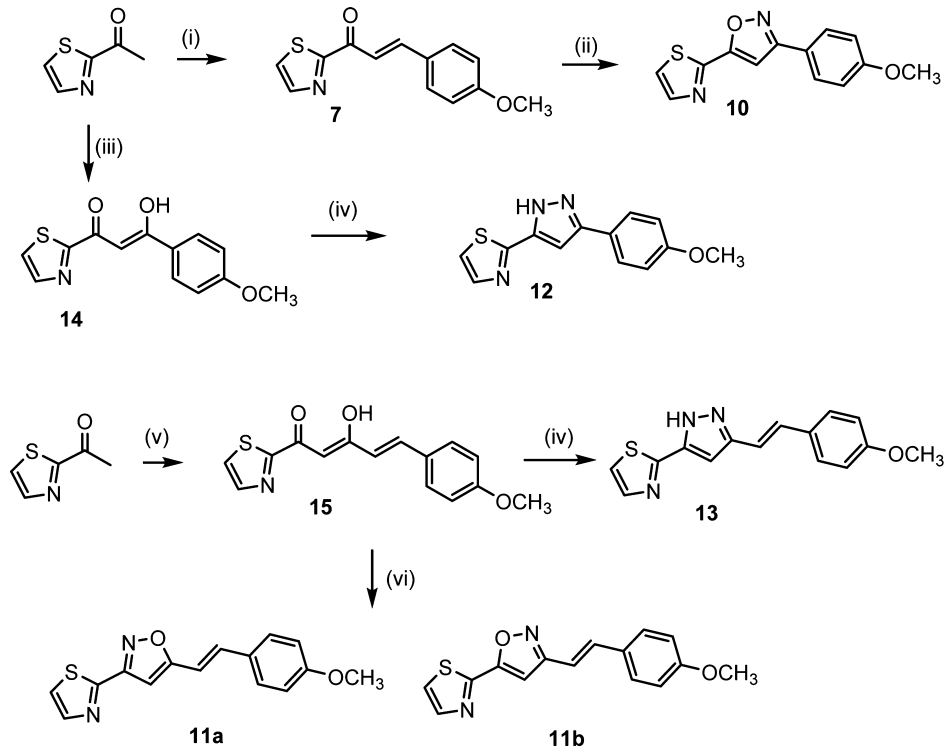

[a]Reagents and conditions: (i) NaOH, CH_3OH; (ii) KOH, CH_3OH, $NH_2OH{\cdot}HCl$/reflux; (iii) NaH, tetrahydrofuran (THF), ethyl-4-methoxybenzoate: (iv) $NH_2NH_2{\cdot}H_2O$, EtOH; (v) trimethylsilane $(TMS)_2NLi$, THF, (E)-3-(4-methoxyphenyl)acryloyl chloride; (vi) NH_2OH−HCl, EtOH, 80 °C.

DOI: 10.1021/acsomega.7b01897
ACS Omega 2018, 3, 4486−4493

Table 3. Three-Dimensional Geometric Characteristics and Chemical Properties from the Minimized Structure of an Individual Compound

#	Ø (°)	ψ (°)	θ (°)	topological diameter (bonds)	accessible surface area (Å^2)	polar surface area (Å^2)	shape attribute
4	−179.2	−36.4	128.1	13.0	529.4	39.7	19.0
5	−179.2	−35.5	128.1	13.0	558.3	32.7	20.0
6	−179.4	−36.2	128.2	13.0	519.0	81.2	20.0
7	−179.2	−36.0	132.5	11.0	459.4	38.7	15.1
8	−179.1	−35.1	132.6	11.0	488.3	32.7	16.1
9	−179.4	−36.0	132.6	11.0	449.0	81.2	16.1
10	−179.9	0.5	151.7	11.0	454.5	43.2	16.1
11b	−179.9	0.4	160.6	13.0	508.9	43.2	18.1
12	−180.0	0.0	150.0	11.0	460.7	46.0	16.1
13	−180.0	0.0	162.8	13.0	514.4	46.0	18.1

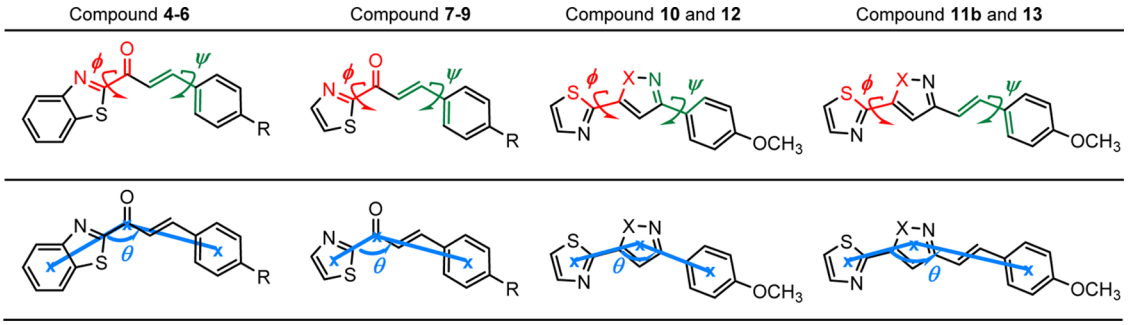

Figure 2. Illustration of the geometric properties of the chalcone and heterocyclic analogues. Red labeled: dihedral angle, Ø; green labeled: dihedral angle, ψ; blue labeled: angle, θ.

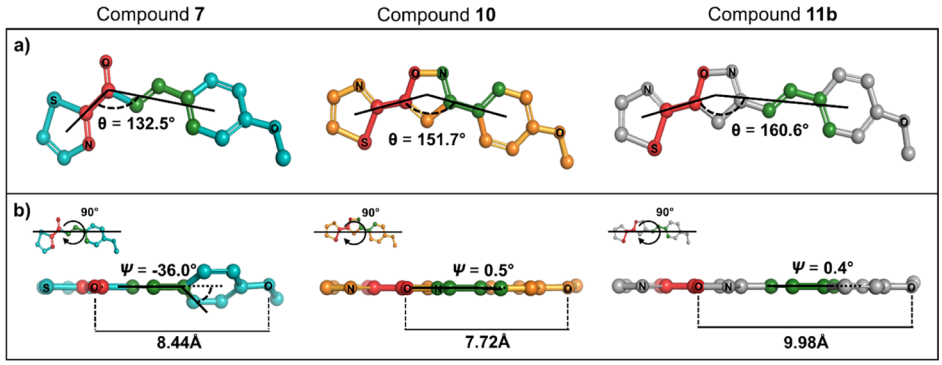

Figure 3. Three-dimensional structures of chalcone compound 7 and isoxazole compounds **10** and **11b**. (a) Compound **11b** shows a flatter angle θ and is closer to linear shape as compared to 7 and **10**. The thiazole ring of compound 7 is in the reverse position to **10** and **11b**. (b) View of 90° rotation of each compound. A dihedral angle ψ = −36.0° is shown in compound 7. Compounds **10** and **11b** were close to flat. The distance of hydrogen bond acceptors from the central group to the methoxy group is 8.44 Å for compound 7, shorter for cyclized compound **10** (7.72 Å), and greater for compound **11b** by the introduced double bond (9.98 Å). Red labeled: dihedral angle Ø. Green labeled: dihedral angle ψ.

corresponding isozazole analogue was obtained as a 50:50 mixture of isomers (**11a**,**b**). In each case, the addition of the double bond resulted in an improvement in affinity for Asyn and A*β* fibrils but not tau fibrils (Table 2). However, both compounds had a 4-5-fold higher selectivity for Asyn versus A*β* fibrils.

Molecular-modeling studies were conducted to identify the molecular properties important for binding to Asyn fibrils. The modeling studies described below were performed on **11b** because subsequent in vitro studies of the tritiated analogue were conducted with this isomer. The structural conformation of **11b** and in vitro binding studies of [^{3}H]**11b** will be reported separately.

The three-dimensional geometric and chemical properties from the minimized structure of each compound are shown in Table 3. The measurement of geometric properties, including dihedral angles Ø and ψ and angle θ are illustrated in Figure 2. A small dihedral angle Ø (−179.1° to −180°) was observed between the central enone/5-member heteroaromatic group and the thiazole/benzothiazole group in compounds **4**−**13**. The dihedral angle ψ for the chalcone series (**4**−**9**, ψ = −35.6° ± 1.1°) was greater than those for the isoxazole and pyrazole analogues (**10**−**13**, ψ = 0.2° ± 0.3°), indicating that the isoxazole and pyrazole analogues are relatively flat compared to the chalcone analogues. The angle θ represents the linearity in shape among the central group and the pendant aromatic groups in each compound. The angle θ for compounds **10**−**13** (θ = 156.3° ± 6.4°) was smaller than that for compounds **4**−**9** (θ = 130.4° ± 2.4°), suggesting that the isoxazole and pyrazole analogues have a more linear geometry relative to the chalcone

DOI: 10.1021/acsomega.7b01897
ACS Omega 2018, 3, 4486−4493

analogues. Overall, the isoxazole and pyrazole analogues are relatively flat and have a more linear geometry relative to the chalcone analogues, resulting in a higher affinity for Asyn fibrils (**10**−**13** K_i = 18.5−162.5 nM vs K_i = 53.0−906.0 nM for **4**−**9**) and a better selectivity for Asyn versus Aβ fibrils (5 to >7 folds for **10**−**13** vs 0 to >9 folds for **4**−**9**).

With respect to substitutions of the phenyl group in the chalcone series, compounds with the dimethylamino group (**5** and **8**) showed a higher accessible surface area (**4** vs **5**: 529.4 vs 558.3 Å^2; **7** vs **8**: 459.4 vs 488.3 Å^2) and a lower polar surface area (**4** vs **5**: 39.7 vs 32.7 Å^2; **7** vs **8**: 38.7 vs 32.7 Å^2) as compared to the compounds with a methoxy group (**4** and **7**). The nitro-containing compounds **6** and **9** have a lower accessible surface area (**6**: 519.0 Å^2, and **9**: 449.0 Å^2) and a higher polar surface area (both **6** and **9** = 81.2 Å^2). Although the accessible and polar surface areas showed a trend in an improved affinity (Table 1) for Aβ fibrils (**4** vs **5**: K_i = 353 vs 91 nM; **7** vs **8**: K_i = >500 vs 505 nM) and a reduced affinity for Asyn fibrils (**4** vs **5**: K_i = 531 vs 906 nM; **7** vs **8**: K_i = 53 vs 96 nM) to the compounds with the methoxy group versus dimethylamino group, the tendency did not consistently show in the nitro-containing compounds. This suggests that these properties may not be good indicators to improve affinity or selectivity for Asyn, Aβ, or tau fibrils.

The isoxazole compound **10**, pyrazole compound **12**, and chalcone compound **7** shared the same topological diameter (i.e., 11 bonds), had a similar shape attribute (**7**, **10**, and **12** = 15.1, 16.1, and 16.1), and a similar range of accessible surface area (**7**, **10**, and **12** = 459.4, 454.5, and 460.7 Å^2). There was a tilt in angle ψ of the benzene ring in **7** (ψ = −36.0°) (Figure 3b), whereas this angle was close to zero in compounds **10** (ψ= 0.5°) and **12** (ψ = 0.0°). The thiazole ring in the minimized structure was in the opposite orientation for chalcone analog **7** relative to the cyclic compounds **10** and **12**. Therefore, the hydrogen bond acceptors or donor (i.e., NH of the pyrazole ring) are located on the same side of **10** and **12**. This may be one of the factors that resulted in the affinity (Table 2) of **10** (K_i = 134 nM) and **12** (K_i = 163 nM) for Asyn fibrils being lower than that of **7** (K_i = 53 nM).

Introduction of a double bond into the isoxazole and pyrazole derivatives increased the accessible surface area (**10** and **12** = 454.5−460.7 Å^2 vs 508.9−514.4 Å^2 for **11b** and **13**) and topological diameter (**10** and **12** = 11.0 bonds vs 13.0 bonds for **11b** and **13**), which resulted in an improvement in affinity for both Asyn (**10** and **12** vs **11b** and **13**, K_i = 134−163 vs 19−59 nM) and Aβ fibrils (**10** and **12** vs **11b** and **13**, K_i = >1000 vs 92−327 nM) (Table 2).

We also observed that the intramolecular distance between hydrogen bond acceptors may be one of the factors influencing the binding affinity to Asyn, that is, for chalcone analog **7**, the distance between the carbonyl oxygen and the oxygen of the methoxy group was 8.44 Å, and its affinity for Asyn was 53 nM. For the isoxazole compound **10**, the distance between the isoxazole oxygen and the oxygen of the methoxy group was shorter at 7.72 Å, and its affinity for Asyn was lower (K_i = 134 nM). The distance between the isoxazole oxygen and the oxygen of the methoxy group in analog **11b** was 9.98 Å, and its affinity for Asyn was 19 nM. Therefore, the rank order potency for binding to Asyn was **11b** > **7** > **10**, which had the same order for distance between the two different oxygen atoms (9.98 > 8.44 > 7.72 Å) (Figure 3b). Ono et al.[15] have studied the different lengths of the double bonds in chalcone analogues; it also showed the different distances between the carbonyl oxygen and the nitrogen of dimethylamino. An extension of the molecular length increased the binding affinity for Asyn fibrils, but no influence for Aβ fibrils, although in our study, the binding affinities for Aβ fibrils were also improved from K_i > 1000 nM (**10**) to K_i = 91.5 nM (**11**) when the intramolecular distance between hydrogen bond acceptors increased. This may be caused by the length differences of the β-sheets in Asyn, Aβ, and tau fibrils. Additionally, it may be due to the binding mode differences between ligands and fibrils. The hydrogen bond may play a more important role in the binding affinity for Asyn than for Aβ or tau fibrils. The observation is based on three of our compounds; more SAR studies and investigation of the interaction between ligands and fibrils are needed for understanding the influence of intramolecular distance between hydrogen bond acceptors.

The results of the molecular-modeling studies indicate that the molecular shape, topographical diameter, and orientation and distance between H-bond acceptors are important in determining the affinity for Asyn fibrils. The studies described above have also led to the identification of a novel compound, **11**, that has a good affinity for Asyn fibrils and a modest selectivity for Asyn versus Aβ fibrils. This compound represents a good lead structure for further SAR studies aimed at the development of a PET radiotracer for imaging Asyn aggregates in vivo with PET. Additional SAR studies of compound **11** are currently ongoing in our group.

EXPERIMENTAL SECTION

Chemistry. Reagents were purchased from Sigma-Aldrich and Fisher Scientific. Silica gel chromatography was carried out on a Biotage Isolera Spektra One chromatograph system. All synthesized compounds were analyzed and confirmed to have purity over 95% with a Waters Alliance LC−MS system. Nuclear magnetic resonance (NMR) spectra were measured on a Bruker 500 or 360 MHz spectrometer, as indicated. Chemical shifts (δ values) were reported in ppm relative to TMS. For multiplicity, s = singlet, d = doublet, t = triplet, and m = multiplet. ^{1}H NMR spectra data are presented as follows: chemical shifts (multiplicity, coupling constants, and integration).

(*E*)-1-(Benzo[*d*]thiazol-2-yl)-3-(4-methoxyphenyl)-prop-2-en-1-one (4).[21] NaOH (60 mg, 1.5 mmol) was dissolved in methanol (5 mL). 4-Methoxybenzaldehyde (150 mg, 1.1 mmol) was added. The mixture was kept stirring at room temperature (rt) for 2 min. 2-Acetylbenzothiazole (177 mg, 1 mmol) was added slowly. The mixture was kept stirring at rt for 15 min, and yellow crystals were formed. The mixture was filtered, and the solid was washed with methanol and hexanes, yielding **4** as yellow crystals (80 mg, 61%). Characterization was the same as reported.[21]

(*E*)-1-(Benzo[*d*]thiazol-2-yl)-3-(4-(dimethylamino)-phenyl)prop-2-en-1-one (5).[22] NaOH (80 mg, 2.0 mmol) was dissolved in methanol (5 mL). 4-*N*,*N*-Dimethylaminobenzaldehyde (300 mg, 2.0 mmol) was added. The mixture was kept stirring at rt for 2 min. 2-Acetylbenzothiazole (177 mg, 1 mmol) was added slowly. The mixture was kept stirring at rt overnight. The red solution was diluted with water (20 mL) and extracted with ethyl acetate (20 mL × 2). The organic layer was dried over Na_2SO_4 and condensed. The residue was purified two times with FC (hexanes/ethyl acetate 10:1−6:1), and compound **5** was obtained as a red solid (50 mg, 17%). ^{1}H NMR (500 MHz, $CDCl_3$): δ 3.07 (s, 6H), 6.72 (d, J = 9.0 Hz, 2H), 7.49−7.58 (m, 2H), 7.67 (d, J = 8.5 Hz, 2H), 7.86 (d, J =

DOI: 10.1021/acsomega.7b01897
ACS Omega 2018, 3, 4486−4493

16.0 Hz, 1H), 7.99, (d, J = 8.0 Hz, 1H), 8.04 (d, J = 16.0 Hz, 1H), 8.21 (d, J = 8.5 Hz, 1H). ^{13}C NMR (126 MHz, $CDCl_3$): δ 40.19, 111.88, 114.79, 122.35, 125.13, 126.68, 127.11, 131.38, 137.36, 147.29, 152.23, 153.80, 169.44, 182.42. MS (ESI) m/z: 309 $(M + H)^+$.

(*E*)-1-(Benzo[*d*]thiazol-2-yl)-3-(4-nitrophenyl)prop-2-en-1-one (6). NaOH (60 mg, 1.5 mmol) was dissolved in methanol (5 mL). 4-Nitrobenzaldehyde (250 mg, 1.66 mmol) was added. The mixture was kept stirring at rt for 2 min. 2-Acetylbenzothiazole (177 mg, 1 mmol) was added slowly. The mixture was kept stirring at rt for 2 h. A slightly yellow solid was formed. The mixture was filtered, and the solid was washed with methanol and then purified with FC (hexanes/ethyl acetate 6:1), yielding compound **6** as slightly yellow crystals (130 mg, 42%). ^{1}H NMR (360 MHz, $CDCl_3$): δ 7.55−7.64 (m, 2H), 7.90 (d, J = 8.3 Hz, 2H), 8.01−8.06 (m, 2H), 8.18−8.31 (m, 4H). ^{13}C NMR (90 MHz, $CDCl_3$): δ 122.52, 124.22, 124.42, 125.60, 127.21, 128.00, 129.49, 142.25, 149.07, 153.85. MS (ESI) m/z: 311 $(M + H)^+$.

(*E*)-3-(4-Methoxyphenyl)-1-(thiazol-2-yl)prop-2-en-1-one (7). NaOH (100 mg, 2.5 mmol) was added to a solution of 4-methoxybenzaldehyde (272 mg, 2 mmol) in methanol (15 mL), and the mixture was stirred for 5 min at 0 °C. 2-Acetylthiazole (254 mg, 2 mmol) was added dropwise in 15 min. The mixture was kept stirring at rt overnight. The mixture was then diluted with H_2O and extracted with ethyl acetate. The organic layer was dried over Na_2SO_4 and condensed. The residue was applied to FC (hexanes/ethyl acetate 3:1), yielding **7** as a slight yellow solid (120 mg, 24%). ^{1}H NMR (500 MHz, $CDCl_3$): δ 3.86 (s, 3H), 6.94 (d, J = 8.8 Hz, 2H), 7.67−7.69 (m, 3H), 7.83 (d, J = 16.0 Hz, 1H), 7.99 (d, J = 16.0 Hz, 1H), 8.05 (d, J = 3.1 Hz, 1H). ^{13}C NMR (126 MHz, $CDCl_3$): δ 55.43, 114.44, 118.12, 126.16, 127.46, 130.85, 144.59, 145.77, 162.10, 169.02, 181.59. MS (ESI) m/z: 246 $(M + H)^+$.

(*E*)-3-(4-(Dimethylamino)phenyl)-1-(thiazol-2-yl)prop-2-en-1-one (8). NaOH (100 mg, 2.5 mmol) was added to a solution of 4-*N*,*N*-dimethylaminobenzaldehyde (300 mg, 2 mmol) in methanol (15 mL), and the mixture was stirred for 5 min at 0 °C. 2-Acetylthiazole (254 mg, 2 mmol) was added dropwise in 15 min. After the addition, the mixture was diluted with H_2O and extracted with ethyl acetate. The organic layer was dried over Na_2SO_4 and condensed. The residue was applied to FC (hexanes/ethyl acetate 5:1), yielding **8** as a slight yellow solid (130 mg, 25%). ^{1}H NMR (500 MHz, $CDCl_3$): δ 3.05 (s, 6H), 6.68 (d, J = 8.5 Hz, 2H), 7.61−7.65 (m, 3H), 7.73 (d, J = 8.0 Hz, 1H), 7.98−8.03 (m, 2H). ^{13}C NMR (126 MHz, $CDCl_3$): δ 40.08, 111.72, 114.98, 122.54, 125.61, 131.14, 144.41, 146.96, 148.72, 152.39, 169.86, 181.34. HRMS m/z (ESI): calcd for $C_{14}H_{15}N_2OS^+$ $[M + H]^+$, 259.0900; found 259.0905.

(*E*)-3-(4-Nitrophenyl)-1-(thiazol-2-yl)prop-2-en-1-one (9). NaOH (160 mg, 4 mmol) was added to a solution of 4-nitrobenzaldehyde (302 mg, 2 mmol) in methanol, and the mixture was stirred for 5 min at 0 °C. 2-Acetylthiazole (254 mg, 2 mmol) was added dropwise in 15 min. After the addition, the mixture was diluted with H_2O and extracted with ethyl acetate. The organic layer was dried over Na_2SO_4 and condensed. The residue was applied to FC (hexanes/ethyl acetate 0−30%), yielding **9** as a slight yellow solid (80 mg, 15%). ^{1}H NMR (500 MHz, $CDCl_3$): δ 7.76 (d, J = 3 Hz, 1H), 7.84 (d, J = 8.5 Hz, 2H), 7.97−8.08 (m, 3H), 8.27 (d, J = 8.5 Hz, 2H). ^{13}C NMR (126 MHz, $CDCl_3$): δ 124.15, 124.53, 127.07, 129.30, 140.65, 142.18, 144.91, 148.72, 167.72, 180.09. MS (ESI) m/z: 261 $(M + H)^+$.

3-(4-Methoxyphenyl)-5-(thiazol-2-yl)isoxazole (10). Compound **7** (50 mg, 0.2 mmol) was dissolved in a solution of KOH in methanol (23 mg in 3 mL). Hydroxylaminium chloride (20 mg, 0.29 mmol) was added. The mixture was kept refluxing for 10 h. The mixture was diluted with ethyl acetate and washed with H_2O and brine. The organic layer was dried over Na_2SO_4 and condensed. The residue was applied to FC (hexanes/ethyl acetate 3:1%), yielding **10** as a slightly brown solid (35 mg, 67%). ^{1}H NMR (500 MHz, $CDCl_3$): δ 3.88 (s, 3H), 7.00−7.02 (m, 3H), 7.49 (d, J = 3.5 Hz, 1H), 7.78 (d, J = 8.5 Hz, 2H), 7.98 (d, J = 3.0 Hz, 1H). ^{13}C NMR (126 MHz, $CDCl_3$): δ 55.43, 96.31, 114.51, 119.76, 120.88, 127.56, 143.69, 158.77, 161.41, 171.09. HRMS m/z (ESI): calcd for $C_{13}H_{11}N_2O_2S^+$ $[M + H]^+$, 259.0536; found, 259.0540.

2-(5-(4-Methoxyphenyl)-1*H*-pyrazol-3-yl)thiazole (12). Sodium hydride (480 mg, 20 mmol) was suspended in THF (2 mL). A solution of ethyl-4-methoxybenzoate (900 mg, 5 mmol) in THF (2 mL) was added, and the mixture was heated to 60 °C. After dropwise addition of a solution of 2-acetylthiozole (254 mg, 2 mmol) in THF (2 mL), stirring was continued for 16 h at 60 °C. The solution was poured into ice-old aqueous HCl (1 M, 25 mL), and the mixture was extracted with dichloromethane (DCM) (20 mL × 2). The organic layer was dried over Na_2SO_4 and condensed under reduced pressure. The residue was applied to FC (DCM/CH_3OH 10:1), yielding **14** as a slightly yellow solid (110 mg, 21%). ^{1}H NMR (500 MHz, $CDCl_3$): δ 3.88 (s, 3H), 6.97 (d, J = 8.5 Hz, 2H), 7.22 (s, 1H), 7.65 (d, J = 3.0 Hz, 1H), 7.98−8.13 (m, 3H), 16.10 (s, 1H). ^{13}C NMR (126 MHz, $CDCl_3$): δ 55.51, 92.04, 114.09, 124.83, 126.49, 129.48, 144.63, 163.60, 166.53, 179.19, 183.01. MS (ESI) m/z: 262 $(M + H)^+$.

Compound **14** (78 mg, 0.3 mmol) was dissolved in ethanol (5 mL), and the mixture was brought to reflux. Hydrazine hydrate (0.5 mL) dissolved in ethanol was added to the refluxed solution. The mixture was kept refluxing for 2 h. The mixture was condensed and partitioned between DCM and water. The organic layer was separated and dried over Na_2SO_4 and then condensed under reduced pressure. The residue was applied to FC (hexanes/ethyl acetate 6:1−3:1), yielding **12** as a colorless solid (45 mg, 58%). ^{1}H NMR (500 MHz, $CDCl_3$): δ 3.83 (s, 3H), 6.92 (d, J = 8.0 Hz, 2H), 7.00 (s, 1H), 7.31 (d, J = 3.0 Hz, 1H), 7.62 (d, J = 8.0 Hz, 2H), 7.86 (d, J = 3.0 Hz, 1H). ^{13}C NMR (126 MHz, $CDCl_3$): δ 55.73, 100.59, 114.38, 118.67, 126.95, 137.94, 143.14, 159.94. MS (ESI) m/z: 258 $(M + H)^+$.

(2*Z*,4*E*)-3-Hydroxy-5-(4-methoxyphenyl)-1-(thiazol-2-yl)penta-2,4-dien-1-one (15). A solution of 1-(thiazol-2-yl)ethan-1-one (1.83 mL, 17.6 mmol) in THF (50.0 mL) was cooled to −78 °C, and 1 M lithium bis(trimethylsilyl)amide in THF (LiHMDS, 19.4 mL, 19.4 mmol) was added dropwise and stirred at −78 °C for 1 h. To the reaction mixture was added (*E*)-3-(4-methoxyphenyl)acryloyl chloride (3.52 g, 21.2 mmol) in THF (20.0 mL) dropwise at the same temperature and stirred at the ambient temperature for 3 h. After the reaction, the reaction mixture was diluted with saturated NH_4Cl (aq) (200 mL) and extracted with EtOAc (150 mL × 2). The combined organic layer was washed with H_2O (200 mL), dried over anhydrous Na_2SO_4, and concentrated. The crude compound was dissolved in methanol and crystallized at 4 °C. The precipitate was filtered and washed with cold methanol which gave **15** (2.40 g, 47%) as a yellow solid. ^{1}H NMR (360 MHz, $CDCl_3$): δ 3.86 (s, 3H), 6.53 (d, J = 15.8 Hz, 1H), 6.75

DOI: 10.1021/acsomega.7b01897
ACS Omega 2018, 3, 4486−4493

(s, 1H), 6.94 (d, J = 8.8 Hz, 2H), 7.53 (d, J = 8.7 Hz, 2H), 7.66 (s, 2H), 7.68 (d, J = 15.8 Hz, 1H), 8.02 (d, J = 3.0 Hz, 1H).

(*E*)-2-(3-(4-Methoxystyryl)-1*H*-pyrazol-5-yl)thiazole (13). To a solution of (2*Z*,4*E*)-3-hydroxy-5-(4-methoxyphenyl)-1-(thiazol-2-yl)penta-2,4-dien-1-one (**15**, 1.00 g, 3.48 mmol) in EtOH (20.0 mL) was added $NH_2NH_2{-}H_2O$ (348 mg, 6.96 mmol) and stirred with reflux at 80 °C for 3 h. The reaction mixture was cooled down to the ambient temperature and EtOH was removed in vacuo. The crude compound was purified by FC (hexanes/ethyl acetate 2:1), which gave **13** (500 mg, 51%) as a yellow solid. ^{1}H NMR (500 MHz, DMSO-d_6): δ 3.77 (s, 3H), 6.91 (s, 1H), 6.95−6.98 (m, 3H), 7.23 (d, J = 16.6 Hz, 1H), 7.49 (d, J = 8.7 Hz, 2H), 7.65 (d, J = 3.2 Hz, 1H), 7.85 (d, J = 3.2 Hz, 1H), 13.31 (s, 1H). ^{13}C NMR (126 MHz, DMSO-d_6): δ 55.16, 100.22, 112.81, 114.32, 119.22, 127.85, 128.80, 130.45, 142.87, 143.05, 146.94, 159.38, 161.69. MS (ESI) m/z: 284 $(M + H)^+$.

(*E*)-3-(4-Methoxystyryl)-5-(thiazol-2-yl)isoxazole and (*E*)-5-(4-Methoxystyryl)-3-(thiazol-2-yl)isoxazole (11). To a solution of (2*Z*,4*E*)-3-hydroxy-5-(4-methoxyphenyl)-1-(thiazol-2-yl)penta-2,4-dien-1-one (**15**, 250 mg, 0.87 mmol) in EtOH (5 mL) was added $NH_2OH{-}HCl$ (121 mg, 1.74 mmol) and stirred at 80 °C for 3 h. The reaction mixture was cooled down to the ambient temperature and EtOH was removed in vacuo. The crude compound was purified by FC (hexanes/ethyl acetate 3:1) which gave an approximately 1:1 mixture of two isomers **11** (80 mg, 32%) as a colorless solid. ^{1}H NMR (500 MHz, DMSO-d_6): δ 3.78 (s, 6H), 6.98 (d, J = 8.7 Hz, 2H), 6.99 (d, J = 8.7 Hz, 2H), 7.08 (s, 1H), 7.13 (d, J = 16.5 Hz, 1H), 7.17 (d, J = 16.5 Hz, 1H), 7.48 (d, J = 16.5, 1H), 7.54 (d, J = 16.5 Hz, 1H), 7.56 (s, 1H), 7.61−7.65 (m, 4H), 7.97 (d, J = 3.1 Hz, 1H), 8.05 (d, J = 3.1 Hz, 1H), 8.08 (d, J = 3.1 Hz, 1H), 8.11 (d, J = 3.1 Hz, 1H). ^{13}C NMR (126 MHz, DMSO-d_6): δ 55.20, 55.25, 98.70, 98.75, 110.45, 112.35, 114.31, 114.38, 122.60, 123.70, 127.78, 128.13, 128.77, 129.01, 135.44, 137.29, 144.06, 144.69, 153.32, 155.46, 158.31, 160.07, 160.33, 162.86, 162.92, 170.38. HRMS m/z (ESI): calcd for $C_{15}H_{13}N_2O_2S^+$ $[M + H]^+$, 285.0692; found, 285.0685.

Binding Assay. The Asyn, Aβ, and tau fibrils used in this study were prepared as previous described.[13] Additional characterization of the Asyn fibril preparation including atomic force microscopy imaging has also been previously reported.[23] Thioflavin-T competition assay studies were also performed following the protocol in a previous paper by Chu et al.[13] In briefly, competition assays used a fixed concentration (1 μM) of Asyn, Aβ, or tau fibrils, consisting of 3 μM, 50 nM, and 4 μM of Thioflavin-T, respectively. The competitor reaction was diluted in 30 mM Tris-HCl, pH 7.4, 0.1% bovine serum albumin and added to the reactions in varying concentrations. The reactions were incubated at room temperature for 1.5 h before quantifying the bound ligand. Fluorescence was determined in a BioTek plate reader using a 440/30 excitation filter and a 485/20 emission filter. Data were analyzed using GraphPad Prism software (version 4.0) to obtain EC_{50} values by fitting the data to the one-site competitive binding equation. K_i values were calculated from EC_{50} values using the equation $K_i = EC_{50}/(1 + [\text{radioligand}]/K_d)$. The average and standard deviation of K_i values were calculated from the results of two competition assays for each fibrils.

Molecular Modeling. All structures were drawn on ChemDraw Profession 15.1 (PerkinElmer Informatics, Inc.) and then imported to Chem3D Ultra 15.1 (PerkinElmer Informatics, Inc.) to minimize individual structures by MMFF94 force field for further geometric characteristic and chemical property measurements. Chem3D Ultra 15.1 program was also applied to measure the chemical properties. Connolly accessible surface area was calculated by the ChemPropStd property module. Polar surface, topological diameter, and shape attribute were measured by the molecular topology property module. Three-dimensional geometric characteristics were measured based on the minimized structures by using Visual Molecular Dynamics program.[24] As illustrated in Figure 2, the dihedral angles $\emptyset$ and ψ between the central group and the pedant aromatic groups were measured to evaluate the torsion degree of each compound. The angle θ among the central group and the pendant aromatic groups was calculated to measure the linearity in shape. A molecular visualization system from open source package, PyMOL (pymol.org), was used for the three-dimensional display.

■ ASSOCIATED CONTENT

Supporting Information

The Supporting Information is available free of charge on the ACS Publications website at DOI: 10.1021/acsomega.7b01897.

Thioflavin-T competition assays for Asyn, Aβ, and tau fibrils (XLSX)

■ AUTHOR INFORMATION

Corresponding Author

*E-mail: rmach@mail.med.upenn.edu (R.H.M.).

ORCID

Chia-Ju Hsieh: 0000-0002-2833-7727

Zhude Tu: 0000-0003-0325-835X

Robert H. Mach: 0000-0002-7645-2869

Present Addresses

∥University of Pennsylvania, Chemistry Building, Room 283, 231 S. 34th St, Philadelphia, PA 19104 (R.H.M., C.-J.H., and K.X.).

⊥Translational Biomarkers, Merck Research Laboratories, West Point, Pennsylvania 19486, United States (T.J.A.G.).

Notes

The authors declare no competing financial interest.

■ ACKNOWLEDGMENTS

Funding for the Michael J. Fox Alpha Synuclein Imaging Consortium was provided by the Michael J. Fox Foundation. The other members of the Michael J. Fox Alpha Synuclein Imaging Consortium include Jamie Eberling, Eugene Johnson, and Kalpana M. Merchant from the Michael J. Fox Foundation; Chester A. Mathis, William E. Klunk, and N. Scott Mason from the University of Pittsburgh Medical Center; Dale Mitchell, Wolfgang Schmidt, and David Hardick from BioFocus—Charles River; Edilio Borroni, Luca Golbi, Michael Horner, and Kevin Nash from Roche; and Joel Mercier from UCB.

■ REFERENCES

(1) Mach, R. H. New targets for the development of PET tracers for imaging neurodegeneration in Alzheimer Disease. *J. Nucl. Med.* **2014**, *55*, 1221−1224.

(2) Mathis, C. A.; Wang, Y.; Holt, D. P.; Huang, G.-F.; Debnath, M. L.; Klunk, W. E. Synthesis and evaluation of 11C-labeled 6-substituted 2-arylbenzothiazoles as amyloid imaging agents. *J. Med. Chem.* **2003**, *46*, 2740−2754.

(3) Mathis, C. A.; Bacskai, B. J.; Kajdasz, S. T.; McLellan, M. E.; Frosch, M. P.; Hyman, B. T.; Holt, D. P.; Wang, Y.; Huang, G.-F.;

DOI: 10.1021/acsomega.7b01897
ACS Omega 2018, 3, 4486−4493

Debnath, M. L.; Klunk, W. E. A lipophilic thioflavin-T derivative for positron emission tomography (PET) imaging of amyloid in brain. *Bioorg. Med. Chem. Lett.* **2002**, *12*, 295−298.
(4) Kung, H. F.; Choi, S. R.; Qu, W.; Zhang, W.; Skovronsky, D. ^{18}F Stilbenes and styrylpyridines for PET imaging of Aβ plaques in Alzheimer's disease: A miniperspective. *J. Med. Chem.* **2010**, *53*, 933−941.
(5) Maruyama, M.; Shimada, H.; Suhara, T.; Shinotoh, H.; Ji, B.; Maeda, J.; Zhang, M.-R.; Trojanowski, J. Q.; Lee, V. M.-Y.; Ono, M.; Masamoto, K.; Takano, H.; Sahara, N.; Iwata, N.; Okamura, N.; Furumoto, S.; Kudo, Y.; Chang, Q.; Saido, T. C.; Takashima, A.; Lewis, J.; Jang, M.-K.; Aoki, I.; Ito, H.; Higuchi, M. Imaging of tau pathology in a tauopathy mouse model and in Alzheimer patients compared to normal controls. *Neuron* **2013**, *79*, 1094−1108.
(6) Xia, C. F.; Arteaga, J.; Chen, G.; Gangadharmath, U.; Gomez, L. F.; Kasi, D.; Lam, C.; Liang, Q.; Liu, C.; Mocharla, V. P.; Mu, F.; Sinha, A.; Su, H.; Szardenings, A. K.; Walsh, J. C.; Wang, E.; Yu, C.; Zhang, W.; Zhao, T.; Kolb, H. C. [^{18}F]T807, a novel tau positron emission tomography imaging agent for Alzheimer's disease. *Alzheimer's Dementia* **2013**, *9*, 666−676.
(7) Chien, D. T.; Szardenings, A. K.; Bahri, S.; Walsh, J. C.; Mu, F.; Xia, C.; Shankle, W. R.; Lerner, A. J.; Su, M. Y.; Elizarov, A.; Kolb, H. C. Early clinical PET imaging results with the novel PHF-tau radioligand [F18]-T808. *J. Alzheimer's Dis.* **2014**, *38*, 171−184.
(8) Hughes, A. J.; Daniel, S. E.; Kilford, L.; Lees, A. J. Accuracy of clinical diagnosis of idiopathic Parkinson's disease: a clinico-pathological study of 100 cases. *J. Neurol., Neurosurg. Psychiatry* **1992**, *55*, 181−184.
(9) Hughes, A. J.; Ben-Shlomo, Y.; Daniel, S. E.; Lees, A. J. What features improve the accuracy of clinical diagnosis in Parkinson's disease: a clinicopathologic study. *Neurology* **1992**, *42*, 1142−1146.
(10) Jankovic, J.; Rajput, A. H.; McDermott, M. P.; Perl, D. P. The evolution of diagnosis in early Parkinson disease. *Arch. Neurol.* **2000**, *57*, 369−372.
(11) Kotzbauer, P. T.; Tu, Z.; Mach, R. H. Current status of the development of PET radiotracers for imaging alpha synuclein aggregates in Lewy bodies and Lewy neurites. *Clin. Transl. Imag.* **2017**, *5*, 3−14.
(12) Kotzbauer, P. T.; Cairns, N. J.; Campbell, M. C.; Willis, A. W.; Racette, B. A.; Tabbal, S. D.; Perlmutter, J. S. Pathologic accumulation of α-synuclein and Aβ in Parkinson disease patients with dementia. *Arch. Neurol.* **2012**, *69*, 1326−1331.
(13) Chu, W.; Zhou, D.; Gaba, V.; Liu, J.; Li, S.; Peng, X.; Xu, J.; Dhavale, D.; Bagchi, D. P.; d'Avignon, A.; Shakerdge, N. B.; Bacskai, B. J.; Tu, Z.; Kotzbauer, P. T.; Mach, R. H. Design, Synthesis, and Characterization of 3-(Benzylidene)indolin-2-one Derivatives as Ligands for alpha-Synuclein Fibrils. *J. Med. Chem.* **2015**, *58*, 6002−6017.
(14) Ono, M.; Watanabe, R.; Kawashima, H.; Cheng, Y.; Kimura, H.; Watanabe, H.; Haratake, M.; Saji, H.; Nakayama, M. Fluoro-pegylated chalcones as positron emission tomography probes for in vivo imaging of beta-amyloid plaques in Alzheimer's disease. *J. Med. Chem.* **2009**, *52*, 6394−6401.
(15) Ono, M.; Doi, Y.; Watanabe, H.; Ihara, M.; Ozaki, A.; Saji, H. Structure-activity relationships of radioiodinated diphenyl derivatives with different conjugated double bonds as ligands for α-synuclein aggregates. *RSC Adv.* **2016**, *6*, 44305−44312.
(16) Volkova, K. D.; Kovalska, V. B.; Balanda, A. O.; Losytskyy, M. Y.; Golub, A. G.; Vermeij, R. J.; Subramaniam, V.; Tolmachev, O. I.; Yarmoluk, S. M. Specific fluorescent detection of fibrillar alpha-synuclein using mono- and trimethine cyanine dyes. *Bioorg. Med. Chem.* **2008**, *16*, 1452−1459.
(17) Yu, L.; Cui, J.; Padakanti, P. K.; Engel, L.; Bagchi, D. P.; Kotzbauer, P. T.; Tu, Z. Synthesis and in vitro evaluation of α-synuclein ligands. *Bioorg. Med. Chem.* **2012**, *20*, 4625−4634.
(18) Bagchi, D. P.; Yu, L.; Perlmutter, J. S.; Xu, J.; Mach, R. H.; Tu, Z.; Kotzbauer, P. T. Binding of the radioligand SIL23 to α-synuclein fibrils in Parkinson disease brain tissue establishes feasibility and screening approaches for developing a Parkinson disease imaging agent. *PLoS One* **2013**, *8*, No. e55031.
(19) Wagner, J.; Ryazanov, S.; Leonov, A.; Levin, J.; Shi, S.; Schmidt, F.; Prix, C.; Pan-Montojo, F.; Bertsch, U.; Mitteregger-Kretzschmar, G.; Geissen, M.; Eiden, M.; Leidel, F.; Hirschberger, T.; Deeg, A. A.; Krauth, J. J.; Zinth, W.; Tavan, P.; Pilger, J.; Zweckstetter, M.; Frank, T.; Bähr, M.; Weishaupt, J. H.; Uhr, M.; Urlaub, H.; Teichmann, U.; Samwer, M.; Bötzel, K.; Groschup, M.; Kretzschmar, H.; Griesinger, C.; Giese, A. Anle138b: a novel oligomer modulator for disease-modifying therapy of neurodegenerative diseases such as prion and Parkinson's disease. *Acta Neuropathol.* **2013**, *125*, 795−813.
(20) Deeg, A. A.; Reiner, A. M.; Schmidt, F.; Schueder, F.; Ryazanov, S.; Ruf, V. C.; Giller, K.; Becker, S.; Leonov, A.; Griesinger, C.; Giese, A.; Zinth, W. Anle138b and related compounds are aggregation specific fluorescence markers and reveal high affinity binding to alpha-synuclein aggregates. *Biochim. Biophys. Acta* **2015**, *1850*, 1884−1890.
(21) Zhu, Y.-P.; Lian, M.; Jia, F.-C.; Liu, M.-C.; Yuan, J.-J.; Gao, Q.-H.; Wu, A.-X. I 2 promoted domino oxidative cyclization for one-pot synthesis of 2-acylbenzothiazoles via metal-free sp 3 C−H functionalization. *Chem. Commun.* **2012**, *48*, 9086−9088.
(22) Rurack, K.; Bricks, J. L.; Reck, G.; Radeglia, R.; Resch-Genger, U. Chalcone-Analogue Dyes Emitting in the Near-Infrared (NIR): Influence of Donor−Acceptor Substitution and Cation Complexation on Their Spectroscopic Properties and X-ray Structure. *J. Phys. Chem. A* **2000**, *104*, 3087−3109.
(23) Dhavale, D. D.; Tsai, C.; Bagchi, D. P.; Engel, L. A.; Sarezky, J.; Kotzbauer, P. T. A sensitive assay reveals structural requirements for alpha-synuclein fibril growth. *J. Biol. Chem.* **2017**, *292*, 9034−9050.
(24) Humphrey, W.; Dalke, A.; Schulten, K. VMD: Visual molecular dynamics. *J. Mol. Graphics* **1996**, *14*, 33−38.

DOI: 10.1021/acsomega.7b01897
ACS Omega 2018, 3, 4486−4493